ELSEVIER

Contents lists available at ScienceDirect

Chemical Engineering Journal

journal homepage: www.elsevier.com/locate/cej





Optimizing alkaline solvent regeneration through bipolar membrane electrodialysis for carbon capture

Sara Vallejo Castaño ^a, Qingdian Shu ^a, Meng Shi ^b, Robert Blauw ^a, Philip Loldrup Fosbøl ^b, Philipp Kuntke ^{a,c,*}, Michele Tedesco ^a, Hubertus V.M. Hamelers ^{a,c}

- ^a Wetsus, European Centre of Excellence for Sustainable Water Technology, Oostergoweg 9, Leeuwarden 8911 MA, the Netherlands
- b Center for Energy Resources Engineering (CERE), Department of Chemical and Biochemical Engineering, Technical University of Denmark, Søltofts Plads Building 228A, Kongens Lyngby, 2800, Denmark
- ^c Environmental Technology, Wageningen University, Bornse Weilanden 9, 6708 WG Wageningen, the Netherlands

ARTICLE INFO

Keywords: Bipolar membrane electrodialysis CO₂ capture Electrochemical solvent regeneration pH-swing

ABSTRACT

This work demonstrates and characterizes the use of a bipolar membrane electrodialysis for pH-driven CO_2 capture and solvent regeneration using potassium hydroxide solutions. The impact of potassium concentration, current density and load ratio on the CO_2 desorption efficiency was analyzed and substantiated with an equilibrium model. The system was tested with partially saturated solutions that mimic the expected carbon content of alkaline solvents that have been in contact with flue gas (carbon loading of 0.6 and K^+ concentration from 0.5 M to 2 M). Among the tested current densities, 1000 A/m^2 demonstrated the highest CO_2 desorption efficiency but also the highest energy consumption, whereas 250 A/m^2 exhibited the lowest energy consumption (8.8 GJ/ton CO_2) but lower CO_2 desorption. Efficiency losses were associated with H^+ transport across the membranes at high load ratios and decrease of the bipolar membranes water dissociation efficiency at low current densities. This work establishes key performance indicators and describes fundamental characteristics of continuous bipolar membrane electrodialysis systems for regeneration of alkaline solvents used in post-combustion CO_2 capture.

1. Introduction

Over the past four decades, the increase of CO₂ concentration in the atmosphere has raised the global average temperature by 1.09 °C above preindustrial levels, changing dramatically the environments we live in. [1] Climate change increases the likelihood and severity of extreme weather events linked to heat such as flooding, wildfires [2], and heatwaves [2–6]; with profound impacts on human- and wildlife across the globe.[7] According to the latest Intergovernmental Panel on Climate Change (IPCC) report, the past decade was "more likely than not" the hottest in the past 125,000 years, and the warming rate of the planet is the largest in 2000 years.[1] Warming is expected to continue at least until mid-century, even if we could make radical changes to decrease the CO₂ concentration in the atmosphere now. In 2015 global leaders agreed to limit global warming below 1.5 °C in the Paris Agreement. Nature restoration, renewable energy generation, electrification, and decarbonization were identified as imminent solutions to be implemented. [8] Particularly, decarbonization is the most cost-effective alternative to reduce CO_2 emissions for industry sectors that heavily rely on fossil fuels such as cement and steel, which together make up to 20% of anthropogenic CO_2 emissions. [9] Thus, we urgently need energy efficient and scalable carbon dioxide capture technologies.

Solvent based CO_2 absorption coupled with thermal regeneration has been widely studied. Monoethanolamine (MEA) is the benchmark for post-combustion carbon capture technology demonstrating an energy consumption of 3.6 to 4 GJ/ton CO_2 (158 to 176 kJ/ mol CO_2) using a thermal regeneration process.[10] More recent developments have achieved reboiler duties of 2.3 GJ/ton CO_2 (88 kJ/mol CO_2) with amines such as 2-Amino-2methyl-propanol (AMP) or piperazine (PZ).[11–13] However, amines are volatile, show moderate toxicity, and suffer from oxidative and thermal degradation, resulting in substantial waste production.[14] Aqueous potassium or sodium hydroxide have emerged as an alternative because they are less volatile, and more resistant to degradation due to their inorganic nature. Thermal regeneration of alkaline CO_2 capture solvents has been demonstrated through causticization with lime, wherein the KOH solvent is regenerated and $CaCO_3$ is

^{*} Corresponding author at: Environmental Technology, Wageningen University, Bornse Weilanden 9, 6708 WG Wageningen, the Netherlands (P. Kuntke). E-mail address: philipp.kuntke@wur.nl (P. Kuntke).

produced. However, regenerating the lime requires the use of high temperatures and natural gas, posing a challenge for technology [15].

As the world moves towards decarbonization, renewable electricity will be more available and affordable. For that reason, electrochemical regeneration of amines and potassium or sodium-based CO2 capture solvents has gained attention in the last years.[15-17] Electrochemical amine regeneration relies on redox-active substances that control the equilibrium of CO₂ in solution. These systems achieved as low as 0.7 GJ/ ton CO₂ (30 kJ/mol CO₂) when operated at current density of 40 A/m². [17] However, they are still in an early stage of development and upscaling pathways are unclear since the process displays high overpotentials at industrially relevant current densities (>250 A/m²). Electrochemically driven potassium carbonate and bicarbonate regeneration and CO2 desorption has also been demonstrated on the lab-scale with H₂-recycling electrochemical cells. In these systems, pH changes are created in the electrochemical cell where CO2 is desorbed at low pH and lean carbon solution is regenerated at high pH. Shu et al. [18] studied solvent regeneration for direct air capture applications, demonstrating an energy consumption of 5.6 GJ/ton CO2 (247 kJ/mol CO2) at 150 A/ m². However, upscaling this system is challenging due to the need to stack adjacent gas-liquid compartments separated by membrane electrode assemblies, and the need for platinum catalyst for H₂ oxidation.

On the other hand, Eiseman et al. demonstrated scalable electrochemical regeneration using bipolar membranes (BPMs), with experimental energy consumptions ranging from 2.3 to 4.5 GJ/ton CO₂ (100 to 200 kJ/mol CO₂) for bicarbonate and carbonate solutions at 50 A/m², respectively.[20] And in theory, Bui et al. estimated that the energy could be reduced to 1.3 GJ/ton CO₂ (60 kJ/mol CO₂).[21] In bipolar membrane electrodialysis (BMED), acid and alkaline compartments are formed by superposing BPMs and cation exchange membranes (CEMs). BPMs dissociate water into protons and hydroxide ions without gas generation, a noticeable advantage compared to water splitting by electrolysis.[22] BPMs have lower cost than membrane electrode assemblies as they do not require expensive platinum catalyst and could have lower overpotential at high current density than gas diffusion electrodes due to their inherently different water dissociation mechanism. Furthermore, BMED systems are commercially available to produce acid and base from inorganic salts such as NaCl, NaNO₃, etc [22], but the technology has not been tested in industrial environments for CO₂ capture and solvent regeneration. Overall, BMED has a large potential for energy consumption optimization, and it provides a rapid upscaling pathway, necessary for the deployment and implementation of carbon capture technologies in the critical opportunity window to curb climate change.

Few papers have studied BMED for CO₂ capture applications. [20,21,23-25] Eiseman et al. analyzed the influence of carbon loading and showed that fully saturated solutions display lower energy consumption and larger efficiency than partially saturated solutions.[20] However, these systems were operated in batch mode, and do not study or report on the regeneration of the solvent, crucial for system integration. Thus, this work aims to characterize a scalable BMED system for pH-driven solvent regeneration of an alkaline absorbent by evaluating the impact of potassium concentration, current density and load ratio on process efficiency, solvent regeneration, and energy consumption in the BMED system. Industrially relevant ranges of current densities (150 to 1000 A/m²) and solvent composition (0.5 to 2 M) were considered for this work. Moreover, a theoretical framework is used to understand and account for efficiency losses associated with species transport across the membranes. By combining advanced bipolar membrane technology with the continuous operation of a CO2 desorption and solvent regeneration process, this research sets a new benchmark that enables seamless integration of existing CO2 capture techniques with advanced solvent regeneration technology for large-scale applications. Thus, this work aims to lay the basis for the future design and development of BMED based technology for CO₂ capture at a larger scale.

2. Materials and methods

2.1. Experimental methodology

The experimental setup is shown in Fig. 1. The electrochemical stack in this work was manufactured by REDstack B.V. (the Netherlands). It consisted of two PMMA end-plates with meshed platinized titanium electrodes (10 g Pt/m², 10 x 10 cm², Evoqua Water Technologies LLC/ Magneto Special Anodes B.V., the Netherlands). In between the endplates, BPMs (Fumasep FBM) and CEMs (Fumasep FKBPK- 130, FUMATECH BWT GmbH, Germany) separated by polymeric spacergaskets of 480 µm thickness (Deukum, Germany) were stacked together to create alternating acidic and alkaline compartments. The stack contained 4 cell pairs, wherein one cell pair is composed of a BPM, a CEM, an acidic and an alkaline compartment. One extra BPM was used as the interface between the alkaline compartment and the anode to sustain the ionic current inside the system. An electrode rinse solution of 0.5 M (mol/L) K₂SO₄ was recirculated in the anode and cathode compartments to convert the electric current into ionic current by oxygen and hydrogen evolution reactions (OER and HER), respectively (Fig. 1).

To operate the system, the rich solvent containing carbonate or bicarbonate ions from the absorption step enters the acidic compartment of the electrochemical regeneration stack, as shown in Fig. 1. In the acidic compartment K⁺ ions transported across the CEM are replaced by H⁺ generated by the BPM decreasing the pH of the solution, resulting in CO₂ evolution. Then, the acidified solution goes through a gas–liquid separation system where high purity CO₂ is recovered. Thereafter, the acidic stream is directed to the alkaline compartment where the solvent is regenerated. There, the acidified solution is replenished with K⁺ crossing the CEM and OH⁻ generated by the BPMs in the alkaline compartment, and can be used again to absorb CO₂.

The experiment was tested with current densities ranging from 150 A/m^2 to $1000 A/m^2$. The flow rate of solution entering the regeneration stack was selected based on the potassium load ratio (L_{K^+}), which is a dimensionless parameter representing the fraction electrical current (or moles of e) to moles of K^+ ions supplied to the system. The load ratio was calculated as

$$L_{K^{+}} = iA_{m}N/\left([K^{+}]_{rich}\dot{V}_{rich}F\right)$$
(1)

where i is the applied current density (A/m^2) , A_m is the active membrane area (0.01 m^2) , N stands for the repeating unit in the stack (four cell pairs), \dot{V}_{rich} is the flow rate of the rich solvent (m^3/s) , $[K^+]_{rich}$ is the molar concentration of total K^+ ions in the rich carbon solution (mol/m^3) to the cell, and F is the Faraday constant (96485 C/mol). Thus, load ratios larger than 1 indicate that more current was supplied to the system than the necessary to remove all the K^+ ions entering the acidic compartment. For a given current density, or potassium concentration of the rich solvent, the load ratio was maintained between 0.5 and 1.2 by varying the flow rate of rich solvent entering the system. The load ratio is widely employed in various electrochemical applications, and it represents a variation of flow rate, with direct implications for the residence time in the system. [19]

2.2. Materials

The composition of the rich solvent used in the experiments simulated the carbon concentration of an alkaline solvent that has been in contact with flue gas in a CO_2 absorption tower. In CO_2 absorption literature [26,27], the carbon loading (α , mol CO_2 / mol K_a^+) is used to measure the extent in which the capacity of the solvent is utilized to store carbon and can be defined for any stream as

$$\alpha = [C_t]/[K_a^+] \tag{2}$$

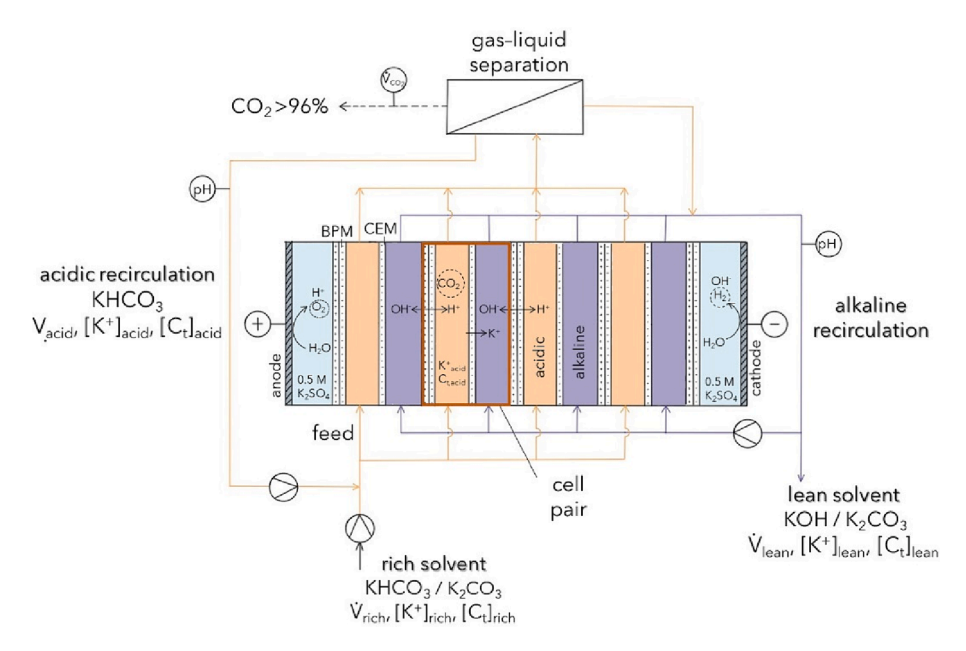


Fig. 1. Schematic representation of BMED experimental setup.

where $[C_t]$ is the concentration of dissolved carbon, and $[K_a^+]$ is the concentration of "active" potassium that can interact with CO₂. The concept of active potassium is analogous to that of alkalinity, as it corresponds to the concentration of anions of the weak acid present in solution (e.g., OH⁻, HCO₃, and CO₃⁻).[28] This is an important distinction since not all the potassium present in solution can interact with CO₂ due to the presence of sulphate as background electrolyte. In other words, the total potassium concentration is the active potassium concentration, plus the concentration of background electrolyte (K_2 SO₄ (aq)).

The rich solvent entering the BMED systems was prepared by mixing potassium carbonate ($K_2\mathrm{CO}_3$) and bicarbonate ($K_1\mathrm{CO}_3$) in constant proportions and varying potassium concentration to maintain a constant carbon loading α_{rich} of 0.6, representative of realistic carbon loadings obtained from CO_2 capture with KOH.[29–31] Following recommendations from previous research, a constant amount of background electrolyte (0.05 M $K_2\mathrm{SO}_4$) was added to all the alkaline solvents to reduce the internal resistance of the cell.[18] Table 1 shows the solution compositions used in the experiments. At least one replicate experiment was performed for solutions with active potassium concentrations of 1 M at 250 $\mathrm{A/m}^2$, 500 $\mathrm{A/m}^2$, and 1000 $\mathrm{A/m}^2$ at load ratio of 0.9. No additional replicate experiments were conducted due to the low variability of the data.

2.3. Experimental equipment

The rich solvent was pumped into the acidic compartment flow using a Simdos 10 liquid dosing pump (1–100 mL/min, KNF, Germany). Internal recirculation in the acidic and alkaline compartments was used to increase the fluid velocity of the fluid inside the compartments (\sim 3 cm/s). Similarly, the electrolyte flow stream was recirculated using a Masterflex L/S peristaltic pump (350 mL/min, Metrohm, the Netherlands). Experiments were carried out in a current density range

Table 1
Concentrations (mol/L) of ions and reagents used in the experiments.

Total K ⁺ [K ⁺]	Active K ⁺ [K _a ⁺]	Total carbon $[C_t]$	[K ₂ CO ₃]	[KHCO ₃]	[K ₂ SO ₄]
0.6	0.5	0.3	0.2	0.1	0.05
1.1	1	0.6	0.4	0.2	0.05
2.1	2	1.2	0.8	0.4	0.05

from 150 A/m^2 to 1000 A/m^2 . Electric power was supplied to the electrochemical stack by a SM3300 Series power supply (Delta Elektronika, the Netherlands). The generated CO_2 was separated from the solution using a 3 M^{TM} Liqui-CelTM EXF-2.5 \times 8 Series membrane contactor (3 M - Liqui-Cel, Germany). To enhance CO_2 desorption, vacuum pressure (-0.4 bar) was applied to the lumen side of the hollow fiber of the membrane contactor using a KNF Liquiport® NF 100 pump.

2.4. Analytical methods

Experiments were performed until reaching a steady-state condition, characterized by a state where the average value of the measured variables was not changing over time (10 min). The potassium and sulfate ion concentrations were measured by taking samples of each stream once steady state had been reached using ion chromatography (761 Compact IC, Metrohm, Switzerland). The total carbon concentration was measured by TIC (TOC-L CPH, Shimadzu BENELUX, 's-Hertogenbosch, the Netherlands). The samples were stored overnight and tested the next day. The samples were diluted by factors in the range of 200 to 800 for TIC analysis and 2500 to 5000 for IC analysis, depending on the solution composition. The pH was measured in both the acidic and alkaline recirculation lines using Memosens sensors (Endress + Hausser B.V., the Netherlands). The pH probes were calibrated prior to every experiment using pH standards of 6, 9, and 13. The sensor data were stored on a data logger (RSG40 datalogger, Endress + Hausser B.V.) and analyzed to find the average values of all the measured variables during steady state. The CO2 flow rate was measured using a MASS-VIEW® model MV-302 flow sensor (Bronkhorst, the Netherlands), and the measured values were based on standard conditions of temperature and pressure (0 °C and 1.01 bar). The purity of CO₂ was checked using gas chromatography (CP-4900, Varian, USA).

2.5. Figures of merit

The removal ratio was used to assess how much potassium or carbon was removed from the influent solution in the acidic compartment, compared to its initial value in the rich solvent. The respective removal ratio of K^+ (R_{K^+}) and carbon (R_{C_t}) was calculated as

$$R_{K^{+}} = \frac{\left([K^{+}]_{rich} - [K^{+}]_{acid} \right)}{[K^{+}]_{rich}}$$
(3)

$$R_{C_t} = \frac{\dot{V}_{CO_2,g}}{\dot{V}_{rich}[C_t]_{rich}V_m} \tag{4}$$

where $[K^+]_{rich}$ and $[K^+]_{acid}$ are the K^+ concentrations in the rich and acidic streams, respectively. $\dot{V}_{CO_2,g}$ is the measured flow rate of CO_2 exiting the regeneration system, \dot{V}_{rich} and $[C_t]_{rich}$ are the influent flow rate and total carbon concentration in the rich stream entering the regeneration system, and $V_m = 22.4 \ L/mol$ is the molar volume of CO_2 in standard conditions (1.01 bar, and 0 °C).

The potassium transport number t_{K+} indicates how much of the current applied to the system was used for potassium transport, and it can be interpreted as the faradaic efficiency of the cell. This parameter was calculated as

$$t_{K+} = \frac{\dot{V}_{rich} \left(\left[K^+ \right]_{rich} - \left[K^+ \right]_{acid} \right) F}{i A_m N} \tag{5}$$

where i is the current density, A_m is the active membrane area, F is the Faraday Constant (96485 C/mol e-) and N is the number of cell pairs. Similarly, the CO₂ desorption efficiency η_{CO_2} indicates how much of the current entering the system was used to desorb CO₂ from the solvent and was calculated as

$$\eta_{CO_2} = \frac{\dot{V}_{CO_2,g}F}{V_m i A_m N} \tag{6}$$

Finally, the specific energy consumption SEC (GJ/ton ${\rm CO_2}$) of regeneration was calculated as

$$SEC_{exp} = \frac{U_{ref} i A_m V_m}{\dot{V}_{CO^{-p}}} \tag{7}$$

where U_{ref} is the reference voltage measured, or voltage across the membranes, measured as the potential difference between two Ag/AgCl reference electrodes placed at the anode and cathode. U_{ref} is different from the total stack voltage as it excludes the contribution of the electrode reactions. This correction was done to differentiate the voltage drop due to electrode reactions to the potential drop of the membranes, since in a large-scale stack the voltage of the electrode reactions is negligible compared to the entire stack voltage that usually contains hundreds of cell pairs.

3. Theoretical framework

A model based on gas-liquid equilibria and mass balances has been developed to simulate the performance of the BMED system. The equilibrium model describes the steady-state conditions of the system with various operating parameters accounting for the following assumptions: i) well-mixed compartments; ii) ideal membrane behavior; iii) absence of transport for neutral species (H₂CO₃) through the membranes.

3.1. Solution equilibrium

The model involves three liquid streams in the system, the influent (rich solvent), the acidic solution, and the alkaline solution (lean solvent). All three liquid streams conform to the acid-base equilibrium according to the dissociation constants of $\rm H_2CO_3$, $\rm HCO_3$, and $\rm H_2O$ (at $25~\rm ^{\circ}C$, $K_{H_2CO_3} = 4.5 \times 10^{-7}~\rm mol/L$, $K_{HCO_3} = 4.7 \times 10^{-11}~\rm mol/L$, and $K_w = 1.0 \times 10^{-14}~\rm mol^2/L^2$). [32,33] Moreover, the charged species (K⁺, H⁺, $\rm HCO_3$, $\rm CO_3^{2-}$, $\rm SO_3^{2-}$, and $\rm OH^-$) comply with the electroneutrality of the solutions. Furthermore, the influent contains a fixed amount of total carbon species that is in accordance with the carbon loading, *i.e.*, the total concentration of $\rm H_2CO_3$, $\rm HCO_3^{-}$, and $\rm CO_3^{2-}$ equals to the product of the carbon loading in the rich solvent and the K⁺ concentration of the solution (Eq. (8).

$$[H_2CO_3]_{rich} + [HCO_3^-]_{rich} + [CO_3^{2-}]_{rich} = \alpha_{rich} \bullet [K_a^+]_{rich}$$
 (8)

where $[H_2CO_3]_{rich}$, $[HCO_3^-]_{rich}$, $[CO_3^{2-}]_{rich}$, and $[K_a^+]_{rich}$ are the concentrations of H_2CO_3 , HCO_3^- , CO_3^{2-} , and active K^+ in the rich solvent.

In the acidic compartment, the solution is in equilibrium with the gas phase in the membrane contactor. According to the partial vacuum applied in the membrane contactor during the experiments, the absolute pressure of gas phase (pure CO_2) is assumed to be 0.6 bar. The dissolved CO_2 concentration ($[H_2\mathrm{CO}_3]_{acid}$) in the acidic solution is determined by the CO_2 partial pressure in the gas based on Henry's Law. In the alkaline compartment, as there is no exchange of CO_2 with other parts of the system, the total concentration of $\mathrm{H}_2\mathrm{CO}_3$, HCO_3^- , and $\mathrm{CO}_3^2^-$ in the alkaline solution remains the same as in the acidic solution.

3.2. Mass transport

In each cell pair, the total flux of cations (K^+ and H^+) across the CEM (J_{tot}) is determined by the applied current density (Eq. (9)).

$$J_{tot} = J_{K^+} + J_{H^+} = \frac{i}{F} \tag{9}$$

where J_{K^+} and J_{H^+} are the molar flux of K^+ and H^+ , respectively. These fluxes are defined by the Nernst-Planck equation (Eqs. (10) and (11)). As the removal of the cations from the acidic compartment are compensated by H^+ produced by the BPM, the transport of K^+ results in a decrease of pH that favors the desorption of CO_2 gas. However, the H^+ transport across the CEM is not intended and reduces the efficiency of the system.

$$J_{K^{+}} = -D_{K^{+}} \bullet \left(\frac{d[K^{+}]}{dx} + [K^{+}]_{m} \frac{d\phi}{dx}\right)$$
 (10)

$$J_{H^{+}} = -D_{H^{+}} \bullet \left(\frac{d[H^{+}]}{dx} + [H^{+}]_{m} \frac{d\phi}{dx}\right) \tag{11}$$

where D_{K^+} and D_{H^+} are the diffusion coefficients of K⁺ and H⁺ in the CEM, respectively, $[K^+]$ and $[H^+]$ represents the K⁺ and H⁺ concentrations at different locations x in the membrane, respectively, $[K^+]_m$ and $[H^+]_m$ are the average concentrations in the membrane, respectively, and ϕ is the dimensionless electric potential obtained by dividing the dimensional potential (V) by RT/F (R is the ideal gas constant and T is the temperature).

As well-mixed compartments are assumed in the model, the ion concentration in the bulk solution is considered equal to the ion concentration on the membrane surface. Moreover, the concentration gradient over the CEM is assumed to be linear to simplify the calculations. Therefore, Eqs. (10) and (11) can be substituted into Eq. (9) to express J_{tot} as a function of J_{K^+} and ion concentrations (Supporting Information).

3.3. Mass balances

As shown in Fig. 1, the rich solvent is first mixed with the acidic solution recirculation before flowing into the acidic compartment. The mixture is acidified for the desorption of CO_2 . The desorbed CO_2 is then separated from the liquid solution in the membrane contactor. After the gas—liquid separation, part of the liquid solution overflows into the alkaline recirculation, while the rest of the liquid recirculates to be mixed with the rich solvent. Finally, the alkaline solution leaves the electrochemical system as the lean solvent to the absorber.

Based on the flow diagram described above, the K^+ mass balance in the system is built in Eqs. (12) – (14). First, the difference between the K^+ concentration in the influent and effluent of the acidic compartment determines the amount of K^+ removed from the compartment, which is proportional to the flux of K^+ over the CEM.

$$J_{K^{+}} = \frac{\dot{V}_{rich}}{A_{m}} \bullet \left([K^{+}]_{rich} - [K^{+}]_{acid} \right)$$
 (12)

Second, the mixing of the rich solvent with the acidic recirculation solution is described in Eq. (13).

$$[K^+]_{mix} \bullet (\dot{V}_{rich} + \dot{V}_{acid}) = [K^+]_{rich} \bullet \dot{V}_{rich} + [K^+]_{acid} \bullet \dot{V}_{acid}$$

$$\tag{13}$$

Where \dot{V}_{acid} is the flow rate of the acidic recirculation solution (excluding the overflow to alkaline recirculation) and $[K^+]_{mix}$ is the K^+ concentration in the mixture of acidic solution and the rich solvent entering the acidic compartment.

Third, considering the electrochemical cell as a control volume, no K^+ is removed or added in the system. Thus, the K^+ concentration in the lean solvent remains the same as in the rich solvent.

$$[K^{+}]_{lean} = [K^{+}]_{rich} \tag{14}$$

The ratio between \dot{V}_{acid} and \dot{V}_{rich} determines the recirculation ratio (λ_r):

$$\lambda_r = \frac{\dot{V}_{acid}}{\dot{V}_{rich}} \tag{15}$$

The λ_r is fixed at 100 in the model to match the experimental conditions. Moreover, the carbon balance in the system can be expressed by Eqs. (16) and (17). The difference of total carbon concentration in the rich solvent and in the acidic solution corresponds to the amount of carbon desorbed from the liquid solution as CO_2 gas, which defines the CO_2 desorption rate (Eq. (16).

$$J_{CO_2} = \frac{\dot{V}_{rich}}{A_m} \bullet ([C_t]_{rich} - [C_t]_{acid})$$
(16)

where J_{CO_2} is the specific CO_2 desorption rate per m^2 of active membrane area (mol/s.m²), and $[C_t]_{acid}$ is the total carbon concentration in the acidic solution.

After CO_2 desorption at the membrane contactor, the liquid solution has no carbon exchange with the environment. Therefore, the total carbon concentration in the lean solvent is the same as in the acidic solution.

$$[C_t]_{lean} = [C_t]_{acid} \tag{17}$$

where $[C_t]_{lean}$ is the total carbon concentration in the lean solvent.

3.4. Energy consumption

The model calculates the specific energy consumption of the system based on the cell voltage, applied current, and molar ${\rm CO_2}$ desorption rate (Eq. (18)).

$$SEC = \frac{U_{cell} \bullet i}{J_{CO_2}} \tag{18}$$

Where U_{cell} is the potential drop over N cell pairs, which is comparable with U_{ref} measured in the experiments. For N cell pairs, the stack consists of N + 1 BPMs, N CEMs, N acidic compartments, and N alkaline compartments. U_{cell} includes the overall potential drop over the BPMs (U_{BPM}) , the CEMs (V_{CEM}) , and the acidic and alkaline solutions (U_{ohmic}) (Eq. (19)).

$$U_{cell} = (N+1) \bullet U_{BPM} + N \bullet U_{CEM} + N \bullet U_{ohmic}$$
(19)

 U_{BPM} is quantified assuming a 14-unit pH difference across the catalytic layer inside the membrane, while each unit of pH gradient implies a potential drop of 59.2 mV of potential drop. U_{CEM} is determined by the K⁺ concentration gradient based on the Nernst equation (Eq. (20)).

$$U_{CEM} = \frac{RT}{F} \ln \frac{[K^+]_{lean}}{[K^+]_{acid}}$$
(20)

The potential drop over the acidic and alkaline solutions are derived from the ohmic losses over the solutions (Eq. (21)).

$$U_{ohmic} = i \bullet (\frac{d_{acidic}}{\sigma_{acidic}} + \frac{d_{alkaline}}{\sigma_{alkaline}})$$
(21)

Where d_{acidic} and $d_{alkaline}$ are the thicknesses of acidic and alkaline compartments (480 μ m each), respectively. σ_{acidic} and $\sigma_{alkaline}$ are the conductivities of the acidic and alkaline solutions, respectively.

In the acidic compartment, CO_2 gas bubbles are formed with the acidification of the solution. The gas bubbles provide extra resistance in the cell as they are not conductive. Therefore, Bruggeman (Eq. (22)), for $\epsilon = 0 - 0.12$) and Maxwell (Eq. (23), for $\epsilon > 0.12$) equations are applied to correct the conductivity of the solutions with gas bubbles.[34]

$$\frac{\sigma_{acidic}}{\sigma_{acidic,0}} = (1 - \epsilon)^{1.5} \tag{22}$$

$$\frac{\sigma_{acidic}}{\sigma_{acidic,0}} = \frac{1 - \epsilon}{1 + \frac{\epsilon}{2}} \tag{23}$$

Where $\sigma_{acidic,0}$ is the conductivity of the acidic solution solely based on liquid phase composition, σ_{acidic} is the corrected conductivity considering the bubble resistance that is applied in Eq. (24), and ϵ is the gas void fraction of CO₂ gas bubbles in the acidic solution. ϵ is defined as the volumetric ratio of CO₂ gas volume (V_g) in the acidic compartment to the total gas and liquid volume ($V_g + V_l$) in the compartment (Eq. (24)).

$$\epsilon = \frac{V_g}{V_v + V_l} \tag{24}$$

Where V_g is calculated based on the total carbon concentration difference between the influent and effluent of the acidic compartment, and V_l is determined by the recirculation flow rate of the acidic solution.

With the calculated composition of the acidic and alkaline solutions, the conductivity $\sigma_{acidic.0}$ and $\sigma_{alkaline}$ are calculated using OLI Studio: Stream Analyzer (ver.10.0, OLI Systems, NJ, USA). Overall, the input for the model includes the composition and flow rate of the rich solvent, and the applied current density. Combining Eqs. (8) – (24), the steady-state conditions of each solution and other figures of merit are solved in Python using Brent's method. [35] According to Eq. (1), the load ratio of K^+ , L_{K^+} , is inversely proportional to the rich solvent flow rate at a constant current density. In the model, the calculations are iterated on a L_{K^+} range between 0.1 and 1.2 with each studied current density. Finally, the model defines the ideal behavior of the electrochemical system. The simulation results can be used to identify the optimal operating conditions of the system, and the gap between the simulation results and the experimental results can help identify losses of performance in practice.

4. Results and discussion

4.1. Increasing current density improves CO₂ desorption efficiency but escalates energy consumption

The effect of current density on critical parameters that define the energy consumption was studied over the range of 150 to 1000 A/m². Fig. 2 shows (a) the corrected stack voltage (U_{ref}) from experiments and model and (b) CO_2 desorption efficiency η_{CO_2} and specific energy consumption (SEC) as a function of current density for experiments conducted at [Ka+] of 1 M, and a load ratio of $L_{K^+} = 0.9$. Fig. 2(a) shows a linear voltage increase with current density, indicating that the stack resistance is constant. The stack resistance was calculated to be 0.01 Ω m² based on the slope of the polarization curve while the value of the intercept corresponds to the open circuit voltage of the system. For completeness, the total stack voltage is shown in Fig. S1. The main contribution to the potential drop of the stack is expected to be the

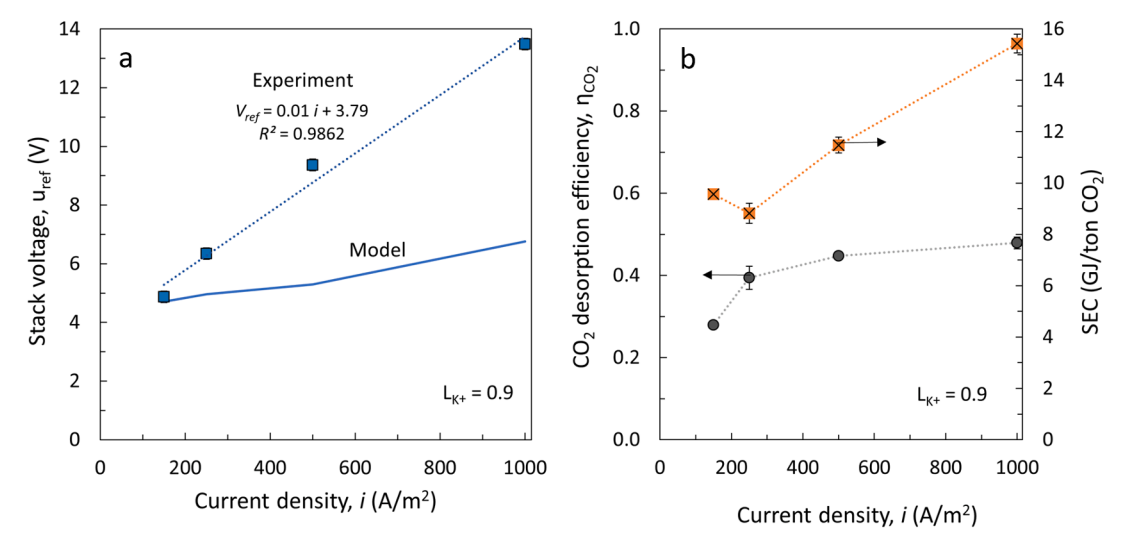


Fig. 2. (a) Simulated and experimental cell pair voltage, (b) process efficiency and specific energy consumption SEC as a function of current density for experiments with $[K_a^+] = 1.0$ M in the rich solvent and, load ratio of $L_{K^+} = 0.9$ and $\alpha_{rich} = 0.6$ (mol CO₂/ mol K_a^+). Error bars at 250 A/m², 500 A/m², and 1000 A/m² obtained from replicate experiments.

BPMs. In this work, the model assumed each BPM adds a potential drop of 0.829 V, which exceeded by one order of magnitude the resistance of the solutions in the acidic and alkaline compartment, and that of the CEMs. At low current density, the theoretical (solid line) and experimental values (points) agreed. However, at high current densities, the measured stack voltage was much larger than the expected theoretical value. There may be several reasons for variations between the model and experimental data. For example, at high current densities concentration gradients between the surface of the membrane and the bulk of the solution, also known as concentration-polarization boundary layers may increase the internal resistance. [19,36] Moreover, the voltage drop estimated by the model is a significant source of deviation from experimental measurements since assuming that the BPM voltage is constant and equal to 0.829 (the thermodynamic potential for water dissociation at a pH difference of 14) is a simplifying assumption. In reality, the BPM voltage increases linearly with current density under the studied region, and voltages up to 1.1 V have been measured for BPM at 1000 A/m² in similar conditions of solution composition. [21] Another hypothesis is that in-situ generated CO₂ bubbles that cover the membrane may cause changes in the current distribution, increasing local current density which led to an increase in potential drop over the membranes.[37] One potential solution is to implement external degassing, which involves adding the rich solvent externally to the acidified solution. By doing so, the formation of CO2 bubbles can be minimized or controlled, which could help to mitigate the increase in potential drop over the membranes. Nevertheless, careful consideration must be given to the tradeoffs and potential efficiency losses associated with this approach, especially concerning H⁺/K⁺ transport competition through the CEM when the pH of the acidic compartment is low. [19.36]

Fig. 2(b) shows that CO_2 desorption efficiency increased with current density, indicating higher water splitting efficiency of the BPMs at higher current densities. This is consistent with literature and manufacturer specifications.[25,38–40] The highest CO_2 desorption efficiency was obtained at $1000~\text{A/m}^2$ for all the solution compositions (Fig. S2). However, at high current density the potential drop was larger resulting in increased energy consumption. The minimum SEC was achieved when operating at a current density of 250 A/m^2 , where the combined effects of internal resistance and ion cross-over were at a minimum. The lowest energy consumption achieved was 8.8 GJ/ton CO_2 at 250 A/m^2 . Above this value, the CO_2 desorption efficiency increased marginally, but the stack voltage increased proportionally to current density, thereby leading to an increase in energy consumption.

Below 250 A/m², although the voltage was low, efficiency losses affected the energy consumption. In this region, the water dissociation efficiency of the BPM decreases, and the current across the BPM can also be transported by potassium or other ions, also known as ion crossover. [41–43] The SEC values observed are in line with previous works. Shu et al. showed a lower energy consumption of ~ 310 kJ/mol CO₂ (7.04 GJ/ton CO₂) at a current density of 200 A/m² with a single cell H₂ recycling system.[18] And, Eisaman et al reported ~ 250 kJ/mol CO₂ (5.68 GJ/ton CO₂) when operating at similar conditions of carbon loading and current density in a batch system, however they did not consider the energy required in the addition of acid to maintain a constant pH in the acidic compartment.[20] It is important to note that partially saturated solutions (e.g. K₂CO₃), require two times more protons to desorb CO2 from the liquid, than fully saturated solutions (e.g. KHCO₃), due to the difference in the ratio of K⁺ to carbonates in the compounds. Therefore, energy consumption could be reduced by at least 40% by using solutions with higher carbon loading.

4.2. Acidic compartment composition dictates CO₂ removal and desorption efficiency

The impact of potassium concentration in the acidic compartment in the BMED system was investigated for different rich solvent influent concentrations. Fig. 3 shows (a) CO₂ removal ratio R_{C_t} and (b) CO₂ desorption efficiency (η_{CO_2}) as a function of load ratio at a constant current density of 1000 A/m². Fig. 3(a) shows that a larger fraction of the CO₂ was removed from the solvent when reaching lower potassium concentration in the acidic compartment ([K⁺]_{acid}), *i.e.*, the CO₂ removal ratio R_{C_t} increased at lower values of [K⁺]_{acid}. As more K⁺ was replaced by H⁺, the pH of the acidic compartment decreased and the speciation of carbon species in solution shifted towards carbonic acid (H₂CO₃), thus releasing more CO₂. Experimental values of CO₂ removal followed the theory closely for all the rich solvent compositions tested.

In contrast, Fig. 3(b) shows that at low $[K^+]_{acid}$, CO_2 desorption efficiency (η_{CO_2}) losses were observed. The maximum CO_2 desorption efficiency achieved was 0.48 for 1 M solutions at a load ratio of 0.9, which is 10 % lower than the corresponding theoretical value. Since operating at low potassium concentration in the acidic compartment $[K^+]_{acid}$ implies high load ratios, concentration gradients between adjacent acidic and alkaline compartments may result in non-ideal effects, such as increased H^+ transport through the CEM or K^+ diffusion through the BPMs, which consume part of the electrical current and do not

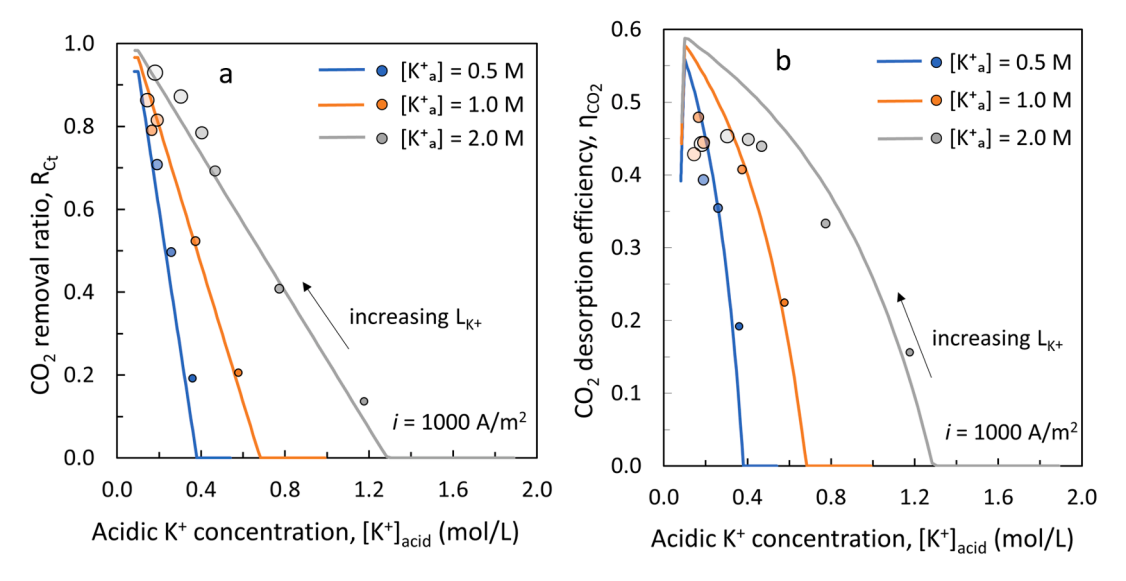


Fig. 3. Experimental and modelled (a) CO_2 removal ratio R_{C_t} and (b) CO_2 desorption efficiency η_{CO_2} as a function of potassium concentration in the acidic compartment ($[K^+]_{acid}$) for different rich solvent $[K^+_a]$ at 1000 A/m². Increasing load ratio indicated with larger symbols and increasing transparency.

contribute to CO_2 desorption.[19,42,43] Taken together, Fig. 3 indicates that most of the carbon that enters the solution is removed when $[K^+]$ in the acidic compartment is low. However, in this condition the CO_2 desorption efficiency was lower than the expected theoretical value, indicating that the lowest $[K^+]_{acid}$ was not the most ideal operating point.

4.3. High load ratios decrease BMED efficiency

To further understand efficiency losses, the potassium concentration and pH in the acidic compartment were plotted as a function of load ratio, as shown in Fig. 4(a) and (b), respectively. Fig. 4(a) shows that the experiments agreed with the model at low load ratios and that $[K^+]_{acid}$ decreased as a function of load ratio. However, Fig. 4(a) and (b) show that at high load ratios, measured values of $[K^+]_{acid}$ and pH were higher than model predictions. The deviations from the model cannot be explained by the transport of H^+ across the CEMs because the model already accounts for it. Thus, the discrepancy between experiments and model could arise from the diffusion of K^+ from the alkaline to the acidic compartment across the BPMs. [42,43] Indeed, at high load ratios the

potassium concentration difference between acidic and alkaline compartment increases (Fig. S3), and the residence time is longer, making transport by diffusion more dominant. The larger [K⁺] in the acidic compartment resulted in discrepancies between model and experimental values of pH in the acidic compartment, as shown in Fig. 4 (b). Thus, unwanted diffusion effects decrease the overall efficiency of the BMED system when operated at high load ratios (L_{K^+}) .

The impact of load ratio (L_{K^+}) on the BMED system performance was investigated for a rich solvent concentration of 1 M $[K_a^+]$ at different current densities. Fig. 5 shows the influence of load ratio on (a) potassium removal ratio (R_{K^+}) , (b) potassium transport number (t_{K^+}) , (c) CO₂ removal ratio (R_{C_t}) , and (d) CO₂ desorption efficiency (η_{CO_2}) . In general, experiments agreed with theoretical trends, and the experiments indicated performance may be current-dependent in the studied ranges. On the other hand, simulation results overlapped for the different current densities evaluated because the model did not consider the BPM's performance dependency on current density. Fig. 5(a) shows that potassium removal ratio R_{K^+} – the ratio of potassium transported across the CEM to the potassium concentration of the rich solvent – increased linearly with the load ratio. The findings agree with the theoretical predictions and

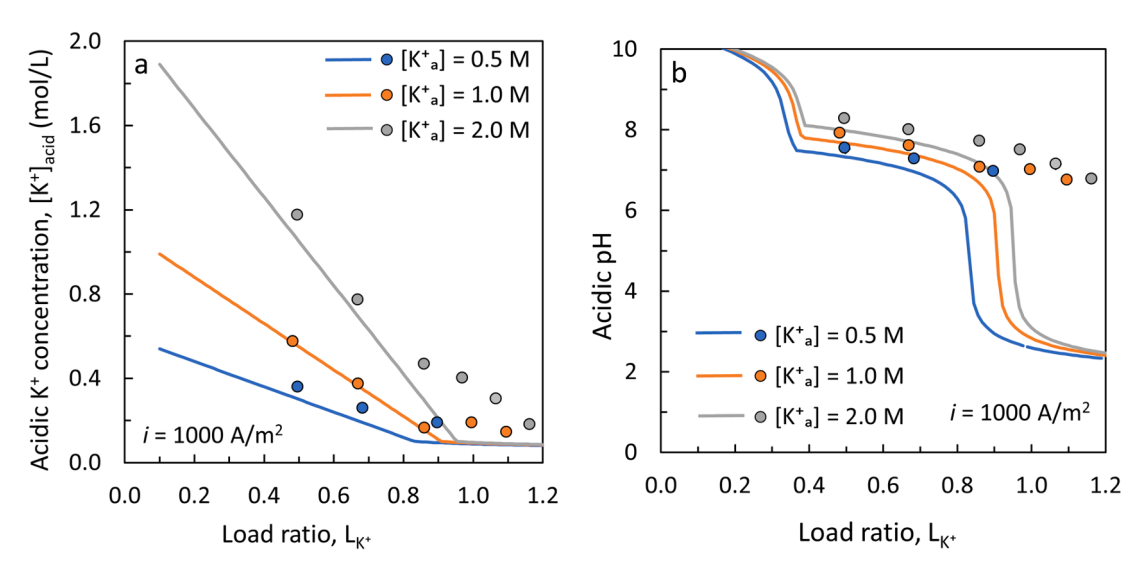


Fig. 4. Experimental and modelled (a) Potassium concentration [K⁺]_{acid} and (b) pH as a function of load ratio in acidic compartment for different rich solvent [K_a⁺].

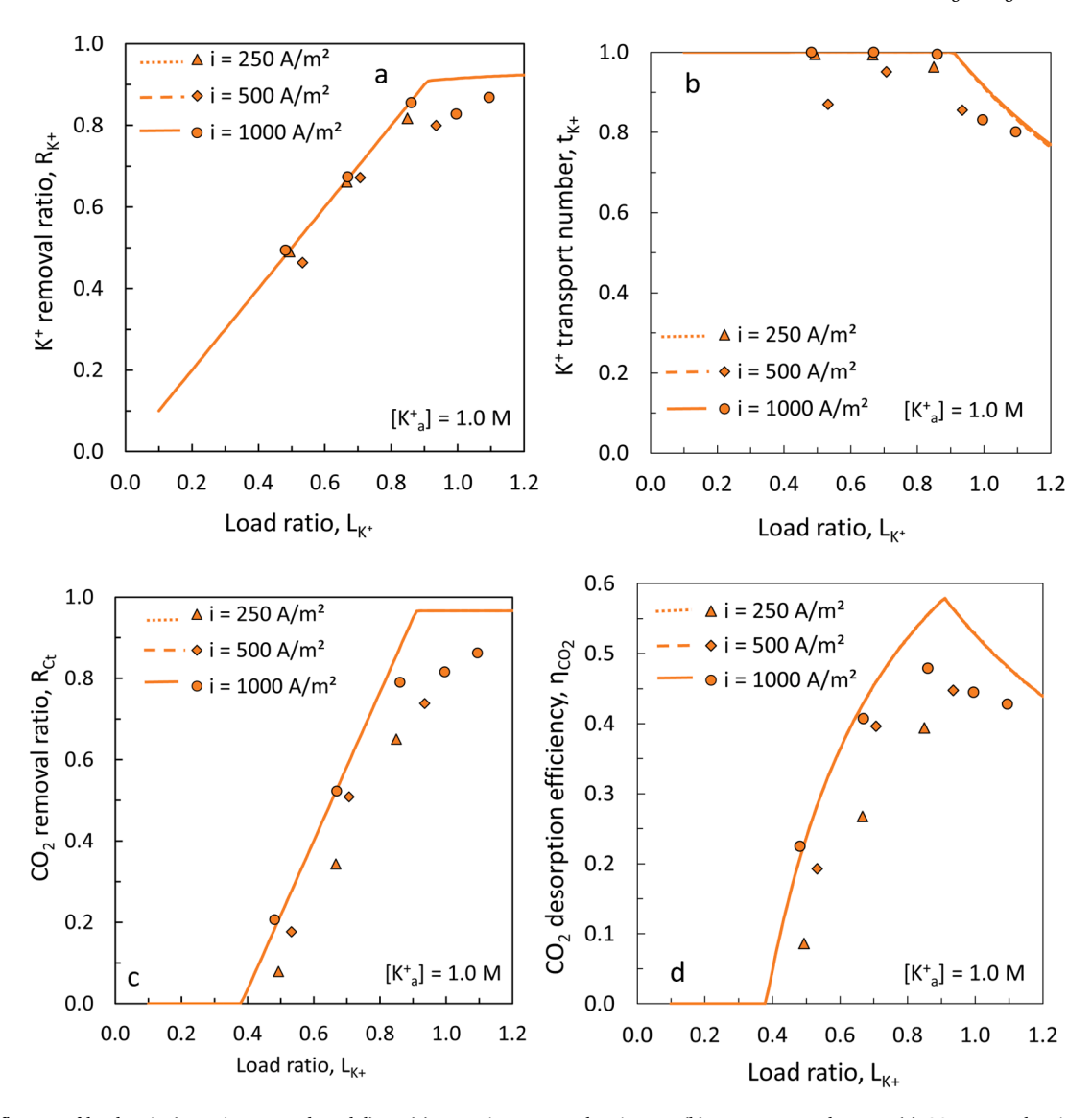


Fig. 5. The influence of load ratio (experiments and model) on (a) potassium removal ratio R_{K^+} , (b) transport number t_{K^+} , (c) CO₂ removal ratio R_{C_i} , and (d) CO₂ desorption efficiency η_{CO_2} for rich solvent concentrations $[K_a^+] = 1.0$ M.

earlier work utilizing the load ratio concept.[19] Similarly, Fig. 5(b) shows that the potassium transport number (t_{K+}) – the ratio of potassium transport across the CEM to the electrical current supplied – was above 0.8 across the studied range, indicative of high faradaic efficiency. Notice that potassium removal (R_{K^+}) is not indicative of faradaic efficiency because current is not involved in the calculation of this parameter, whereas potassium transport number (t_{K+}) is a direct indication of the faradaic efficiency of the system because it compares potassium transport with current supplied. When operating at load ratios larger than 1, more current is supplied to the system than the amount of potassium available for transport, and in this condition, unwanted transport effects such as counter-ion transport of [H⁺] across the CEM start to become more prominent. That explains why at load ratios larger than 0.9, the model predicts a decrease in the potassium transport number, whereas in that same range potassium removal R_{K^+} plateaus.

Removal ratio and efficiency parameters were also defined for CO_2 , as shown in Fig. 5(c) and (d). Analogous to Fig. 5(a), (c) demonstrates that CO_2 removal increased linearly with load ratio, and it plateaued after $L_{K^+}=0.9$. Fig. 5(d) shows that CO_2 desorption efficiency reached a maximum in the same operating condition and decreased thereafter. At load ratios below 0.9, CO_2 removal ratio and desorption efficiency were limited by the solution composition and potassium removal. When

operating with a partially saturated solvent ($\alpha_{rich} = 0.6$) at low load ratios potassium removal is low (Fig. 5a), resulting in high pH in the acidic compartment (Fig. S4). In these conditions, CO2 can hardly be desorbed because the liquid-vapor equilibrium of this component is directly related to the presence of H₂CO₃ in solution, which is absent from solutions with high pH. Thus, CO₂ desorption efficiency increased as more potassium was removed from solution, reached a maximum when the load ratio was equal to 0.9 and decreased thereafter due to the thermodynamic limitations of transporting K⁺ across the CEM in a K⁺ depleted solution against the concentration gradient. The maximum CO2 desorption efficiency was theoretically limited by the carbon loading of the rich solvent (α_{rich}) – i.e., a fully saturated solution has a maximum theoretical CO₂ desorption efficiency of 1 – highlighting the importance of achieving the highest possible carbon loading during the absorption step to maximize faradaic efficiency during CO_2 desorption. The findings are consistent with previous literature [20] and were equivalent for all solution compositions tested (Figs. S5 and S6). Interestingly, although potassium removal and transport number were close to model predictions, CO₂ removal and desorption efficiency displayed larger deviations. The CO₂ desorption rate could have been impacted by low residence times in the liquid/gas separator, by gas leaks in the system at high current densities, and by the accuracy of the flow meter at low CO2

desorption flow rates (<50 mL/min). Additionally, the low residence time of the liquid in the membrane contactor may have inhibited $\rm CO_2$ desorption. Overall, the results in Fig. 5 indicate that experimental carbon removal followed the trend of theoretical calculation and that more carbon removal was achieved at high load ratios at the expense of lower $\rm CO_2$ desorption efficiency.

4.4. Optimal solvent composition is a function of load ratio and current density

The combined effects of current density and solvent concentration on CO₂ desorption efficiency were evaluated as a function of load ratio. Fig. 6 shows CO₂ desorption efficiency as a function of load ratio for 0.5 M, 1 M and 2 M solutions for current densities of (a) 250 A/m^2 , (b) 500 A/m^2 A/m^2 , and (c) 1000 A/m^2 . In general, the experimental performance of the BMED stack with all solutions operating at 250 A/m² was less optimal than those at higher current density. At this current density, the CO₂ production flow rate remained consistently below 50 mL/min across all experiments (Fig. 7a). At this low flow rate experimental error could account for up to 20% of the measurement, leading to larger deviations between the model and experimental measurements. Moreover, experiments showed that 2 M solutions, with the highest KOH concentration, displayed the lowest performance of all solution compositions when tested at low current densities, but their efficiencies improved with increasing current density. In Fig. 6(c), at current density of 1000 A/m² and load ratios larger than 0.9, 1 M and 2 M solutions showed similar CO₂ desorption efficiency. The dependency of solution composition and current density on efficiency is consistent with literature that indicates that solutions with higher ion concentration suffer from low faradaic efficiency due to ion leakage across the BPMs, but this effect is reduced at high current density. [38,42,43] Potassium transport number results provide similar insights (Fig. S7). The interaction effects between current density and solvent concentration are not reflected in the theoretical predictions because non-ideal transport effects such as ion crossover across the BPMs are not accounted for in the model. Note that the maximum CO₂ desorption efficiency predicted increased with solvent concentration and was reached at increasingly larger load ratios. Indeed, solutions with higher K⁺ concentration still contain significant potassium and carbonates in the acidic compartment, providing more buffer capacity. Thus, the theory suggests that at high load ratios solutions with larger K⁺ concentration and larger K⁺ to H⁺ ratio than more diluted solutions show improved potassium transport numbers and CO₂ desorption efficiency. Interestingly, 1 M solutions displayed better performance than 0.5 M solutions, contrasting with findings from previous research. In this case, it is possible that the dehydration of carbonic acid $(CO_2(aq) + H_2O \leftrightarrow H_2CO_3)$ with a characteristic reaction time of 0.05 s [44] could impact the $\rm CO_2$ desorption for 0.5 M solutions because their residence time is lower than 1 and 2 M solutions at the same load ratio and current density. This highlights that solution composition, current density, and load ratio conditions display strong interaction effects in BMED systems. [38,45]

4.5. CO₂ desorption rate, solvent regeneration, and energy consumption

Fig. 7 shows the effect of load ratio on (a) the CO₂ desorption rate, (b) carbon loading of the lean solvent, and (c) the specific energy consumption (SEC) for all compositions and current densities tested. Fig. 7 (a) demonstrates that CO₂ desorption rate increased by a factor of 4 with current density from 250 to 1000 A/m², as expected from the fourfold increase in current density, which is expected to desorb more CO2. Nevertheless, experimental CO2 desorption rates were always lower than model predictions, which was in line with the efficiency losses observations from previous sections. The model predicted that CO₂ desorption rate should peak at a load ratio between 0.8 and 1 depending on solution composition. This peak efficiency, Fig. 7(a), was achieved when the ratio of "active potassium" to total potassium ($[K_a^+]/[K^+]$) was equivalent to the load ratio. The decline in desorption rate after the peak was related to a reduced transport number and lower availability of carbon in the rich solvent, in accordance with previous research.[19] For 2 M [K₂] rich solvent compositions, the experimental CO₂ desorption rate did not display a peak as that of the model in the investigated range, but rather reached a plateau at high load ratios. This could be attributed to the discrepancies between theory and experiments observed for K⁺ removal at high load ratios (Fig. S6). A decrease in performance is expected to occur at load ratios larger than 1.2.

Fig. 7(b) shows that the load ratio dictates the degree of solvent regeneration and lean carbon loading of the regenerated solvent, highlighting the importance of this operational parameter as a tool to refine the process output. Depending on the load ratio, the electrochemical system decreased the carbon loading of the solution from 0.6 to 0.1. The maximum solvent regeneration – calculated as the lean carbon loading divided by the rich carbon loading ($\alpha_{lean}/\alpha_{rich}$)- was 83 % and was achieved at high load ratios ($L_{K^+} > 0.9$). Finally, Fig. 7(c) shows that for all solution compositions tested, the lowest SEC was achieved when operating at 250 A/m² and a load ratio of 0.9. The lowest energy consumption was achieved for 1 M solutions with a value of 8.8 GJ/ton, followed by 0.5 M (10 GJ/ton CO₂) and 2 M solution (11 GJ/ton CO₂). It is important to note that although 2 M solutions are detrimental to the system performance under certain conditions, these solutions would be beneficial for CO₂ capture due to their higher absorption capacity, i.e., a 2 M solution can desorb twice as much CO₂ per m³ of solution than 1 M solutions. An advantage of using a more concentrated solution would be

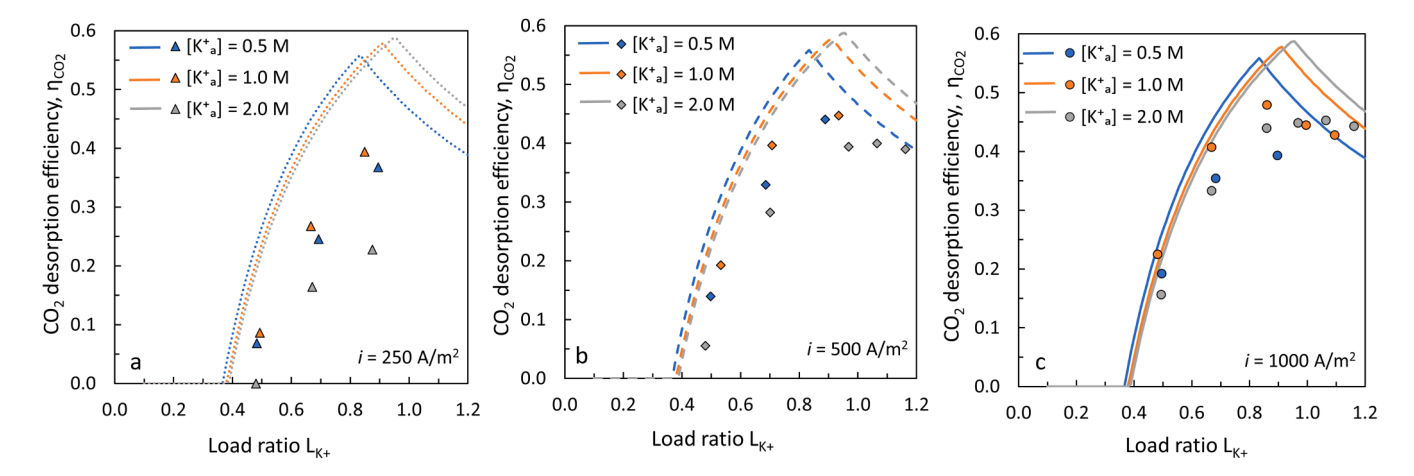


Fig. 6. Experimental and modelled CO₂ desorption efficiency as a function of load ratio for rich solvents with [K_a⁺] of 0.5 M, 1 M and 2 M at current densities of (a) 250 A/m², (b) 500 A/m², and (c) 1000 A/m².

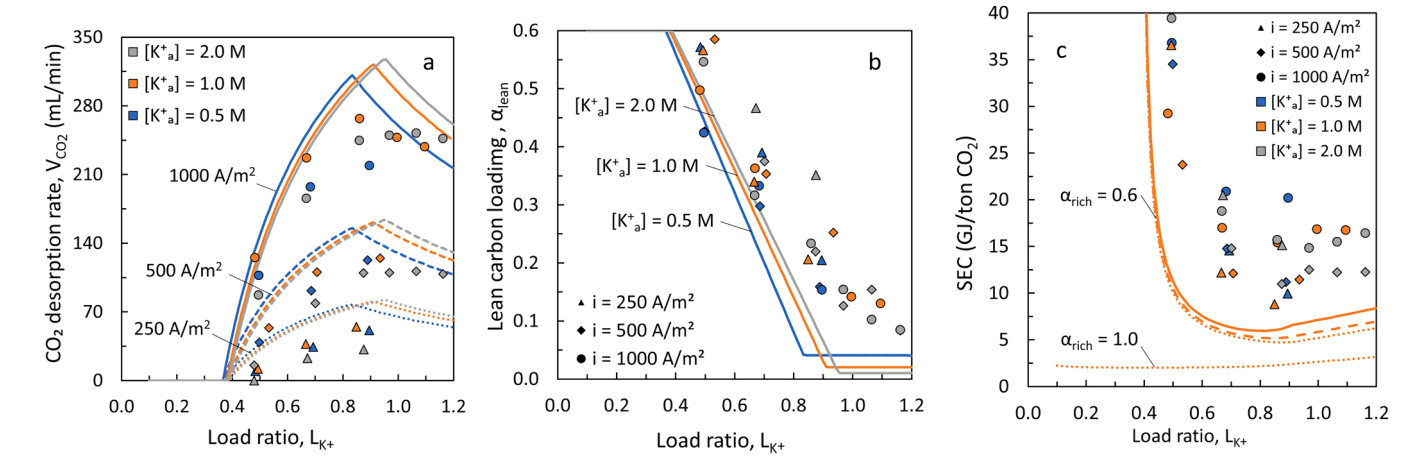


Fig. 7. Experimental (data points) and modelled (lines) effect of load ratio on (a) the CO_2 desorption rate, (b) lean carbon loading of the regenerated solvent, and (c) the specific energy consumption (SEC) as for all compositions and current densities tested. Blue, orange and grey colors indicate $[K_a^+]$ of 0.5 M, 1 M, and 2 M, respectively. Current density data points and model results are shown as triangles, diamonds and circles, and by dotted, dashed, and solid lines, for 250 A/m², 500 A/m², and 1000 A/m², respectively. (For interpretation of the references to colour in this figure legend, the reader is referred to the web version of this article.)

that the volume of the plant, which is directly related to capital expenditure (CAPEX) could be substantially reduced. However, the optimal concentration for the integrated CO_2 absorption and regeneration must balance CO_2 capture efficiency, desorption efficiency, and CAPEX considerations.

5. Conclusion

This study evaluated the performance of Bipolar Membrane Electrodialysis (BMED) for CO₂ desorption and solvent regeneration from an enriched alkaline absorbent based on KOH. A comprehensive analysis of the experimental results was achieved by comparing them with an equilibrium model. The experimental findings align closely with model predictions. The method employed for data analysis successfully distinguished between CO₂ desorption efficiency and faradaic efficiency, providing valuable insights into performance losses associated to transport phenomena across CEMs and BPMs. Further analysis indicated that high rich solvent concentrations, low current densities, and high load ratios exacerbated inefficiencies from unwanted K⁺ transport at across the BPMs. To improve the accuracy of the model, adjustments should be made to account for non-ideal behavior of BPMs.

The 1 M solutions exhibited the best performance at a load ratio of 0.9. Nevertheless, the optimal load ratio changed with solution composition and depended on the ratio of active potassium and background electrolyte. The lowest energy consumption achieved in this study was 8.8 GJ/ton $\rm CO_2$. Among the tested current densities, $1000~\rm A/m^2$ demonstrated the highest $\rm CO_2$ desorption efficiency but also the highest energy consumption, whereas 250 A/m² exhibited the lowest energy consumption but lower desorption efficiency. The maximum theoretical desorption efficiency could not be achieved in any case, thus further investigation in this topic is required to improve energy consumption. Future work should aim to reduce internal resistance at high current density and increase water splitting efficiency at low current densities.

In summary, this study sheds light on the effectiveness and limitations of BMED in achieving efficient CO_2 desorption. The results in this study demonstrate a significant development in the field of electrochemically driven CO_2 capture, as they are the first steady state study combining simultaneous CO_2 desorption and solvent regeneration in a scalable multicompartment system. The findings offer valuable insights for optimizing the technology, identify optimization pathways and have direct implications in real-life applications of carbon capture using pH driven electrochemical systems for solvent regeneration.

CRediT authorship contribution statement

Sara Vallejo Castaño: Writing – review & editing, Writing – original draft, Supervision, Methodology, Investigation, Formal analysis, Data curation, Conceptualization. Qingdian Shu: Writing – review & editing, Visualization, Validation, Software, Investigation, Conceptualization. Meng Shi: Writing – review & editing. Robert Blauw: Investigation. Philip Loldrup Fosbøl: Writing – review & editing. Philipp Kuntke: Writing – review & editing, Validation, Supervision, Resources, Project administration, Methodology, Funding acquisition. Michele Tedesco: Writing – review & editing, Supervision, Resources, Funding acquisition, Formal analysis, Conceptualization. Hubertus V.M. Hamelers: Methodology, Supervision, Writing – review & editing.

Declaration of competing interest

The authors declare that they have no known competing financial interests or personal relationships that could have appeared to influence the work reported in this paper.

Data availability

The research data underlying this work will be available at: 10.4121/3c24cd14-e0fc-4b66-802d-3315ffc4fffa

Acknowledgements

The authors would like to thank ConsenCUS project for providing financial support. The project leading to this application has received funding from the European Union's Horizon 2020 research and innovation programme under grant agreement No 101022484. This work was partially performed in the cooperation framework of Wetsus, European Centre of Excellence for Sustainable Water Technology (www. wetsus.eu). Wetsus is co-funded by the Dutch Ministry of Economic Affairs and Ministry of Infrastructure and Environment, the European Union Regional Development Fund, the Province of Fryslan, and the Northern Netherlands Provinces. S.V.C., Q.S., M.T. P.K., and H.V.M.H. would like to thank the participants of the research theme "Sustainable Carbon Cycle" for fruitful discussions and financial support.

Appendix A. Supplementary data

Supplementary data to this article can be found online at https://doi.org/10.1016/j.cej.2024.150870.

References

- In-depth Q&A: The IPCC's sixth assessment report on climate science Carbon Brief, (n.d.). https://www.carbonbrief.org/in-depth-qa-the-ipccs-sixth-assessment-report-on-climate-science/ (accessed April 18, 2023).
- [2] L.R. Hawkins, J.T. Abatzoglou, S. Li, D.E. Rupp, Anthropogenic Influence on Recent Severe Autumn Fire Weather in the West Coast of the United States, Geophys. Res. Lett. 49 (2022), https://doi.org/10.1029/2021GL095496.
- [3] L.J. Harrington, K.L. Ebi, D.J. Frame, F.E.L. Otto, Integrating attribution with adaptation for unprecedented future heatwaves, Clim. Change 172 (2022), https://doi.org/10.1007/S10584-022-03357-4.
- [4] S.C. Herring, M.P. Hoerling, J.P. Kossin, T.C. Peterson, P.A. Stott, Explaining extreme events of, from a climate perspective, Bull. Am. Meteorol. Soc. 96 (2015) (2014) S1–S172, https://doi.org/10.1175/BAMS-EXPLAININGEXTREMEEVENTS2014.1.
- [5] M. Marcos, A. Amores, Quantifying anthropogenic and natural contributions to thermosteric sea level rise, Geophys. Res. Lett. 41 (2014) 2502–2507, https://doi. org/10.1002/2014GL059766.
- [6] F. Otto, Attribution of extreme weather events: how does climate change affect weather? Weather 74 (2019) 325–326, https://doi.org/10.1002/WEA.3610.
- [7] C. Raymond, T. Matthews, R.M. Horton, The emergence of heat and humidity too severe for human tolerance, Sci. Adv. 6 (2020), https://doi.org/10.1126/SCIADV. AAW1838.
- [8] K. Dooley, Z. Nicholls, M. Meinshausen, Carbon removals from nature restoration are no substitute for steep emission reductions, One Earth 5 (2022) 812–824, https://doi.org/10.1016/j.oneear.2022.06.002.
- [9] T.A. Napp, A. Gambhir, T.P. Hills, N. Florin, P.S. Fennell, A review of the technologies, economics and policy instruments for decarbonising energy-intensive manufacturing industries, Renew. Sustain. Energy Rev. 30 (2014) 616–640, https://doi.org/10.1016/j.rser.2013.10.036.
- [10] M. Bui, C.S. Adjiman, A. Bardow, E.J. Anthony, A. Boston, S. Brown, P.S. Fennell, S. Fuss, A. Galindo, L.A. Hackett, J.P. Hallett, H.J. Herzog, G. Jackson, J. Kemper, S. Krevor, G.C. Maitland, M. Matuszewski, I.S. Metcalfe, C. Petit, G. Puxty, J. Reimer, D.M. Reiner, E.S. Rubin, S.A. Scott, N. Shah, B. Smit, J.P.M. Trusler, P. Webley, J. Wilcox, N. Mac Dowell, Carbon capture and storage (CCS): The way forward, Energy, Environ. Sci. 11 (2018) 1062–1176, https://doi.org/10.1039/
- [11] A. Gladis, M.T. Gundersen, P.L. Fosbøl, J.M. Woodley, N. von Solms, Influence of temperature and solvent concentration on the kinetics of the enzyme carbonic anhydrase in carbon capture technology, Chem. Eng. J. 309 (2017) 772–786, https://doi.org/10.1016/j.cej.2016.10.056.
- [12] P. Brandl, M. Bui, J.P. Hallett, N. Mac Dowell, A century of re-exploring CO2 capture solvents, International Journal of Greenhouse Gas Control 120 (2022), https://doi.org/10.1016/j.ijggc.2022.103771.
- [13] E. Sanchez Fernandez, E.L. V Goetheer, G. Manzolini, E. Macchi, S. Rezvani, T.J.H. Vlugt, Thermodynamic assessment of amine based CO 2 capture technologies in power plants based on European Benchmarking Task Force methodology, Fuel 129 (2014) 318–329. 10.1016/j.fuel.2014.03.042 (accessed September 18, 2023).
- [14] K.S. Zoannou, D.J. Sapsford, A.J. Griffiths, Thermal degradation of monoethanolamine and its effect on CO2 capture capacity, Int. J. Greenhouse Gas Control 17 (2013) 423–430, https://doi.org/10.1016/j.ijggc.2013.05.026.
- [15] F. Sabatino, M. Mehta, A. Grimm, M. Gazzani, F. Gallucci, G.J. Kramer, M., Van Sint Annaland, Evaluation of a Direct Air Capture Process Combining Wet Scrubbing and Bipolar Membrane Electrodialysis, Ind. Eng. Chem. Res. 59 (2020) 7007–7020, https://doi.org/10.1021/acs.iecr.9b05641.
- [16] G.H. Choi, H.J. Song, S. Lee, J.Y. Kim, M.W. Moon, P.J. Yoo, Electrochemical direct CO2 capture technology using redox-active organic molecules to achieve carbonneutrality, Nano Energy 112 (2023), https://doi.org/10.1016/j.
- [17] T.L. Biel-Nielsen, T.A. Hatton, S.N.B. Villadsen, J.S. Jakobsen, J.L. Bonde, A. M. Spormann, P.L. Fosbøl, Electrochemistry-Based CO2 Removal Technologies, ChemSusChem 16 (2023), https://doi.org/10.1002/cssc.202202345.
- [18] Q. Shu, C.S. Sin, M. Tedesco, H.V.M. Hamelers, P. Kuntke, Optimization of an electrochemical direct air capture process with decreased CO2 desorption pressure and addition of background electrolyte, Chem. Eng. J. 470 (2023) 144251, https:// doi.org/10.1016/j.cej.2023.144251.
- [19] Q. Shu, L. Legrand, P. Kuntke, M. Tedesco, H.V.M. Hamelers, Electrochemical Regeneration of Spent Alkaline Absorbent from Direct Air Capture, Environ. Sci. Tech. 54 (2020) 8990–8998, https://doi.org/10.1021/acs.est.0c01977.
- [20] M.D. Eisaman, L. Alvarado, D. Larner, P. Wang, B. Garg, K.A. Littau, CO2 separation using bipolar membrane electrodialysis, Energy, Environ. Sci. 4 (2011) 1319–1328, https://doi.org/10.1039/c0ee00303d.
- [21] J. Bui, E. Lucas, E.W. Lees, A.K. Liu Jr., H.A. Atwater, C. Xiang, A.T. Bell, A. Z. Weber, Analysis of bipolar membranes for electrochemical CO2 capture from air and oceanwater, Energ. Environ. Sci. (2023), https://doi.org/10.1039/ D3EE014069.
- [22] R. Pärnamäe, S. Mareev, V. Nikonenko, S. Melnikov, N. Sheldeshov, V. Zabolotskii, H.V.M. Hamelers, M. Tedesco, Bipolar membranes: A review on principles, latest

- developments, and applications, J Memb Sci 617 (2021), https://doi.org/10.1016/i.memsci.2020.118538.
- [23] M.D. Eisaman, L. Alvarado, D. Larner, P. Wang, K.A. Littau, CO 2 desorption using high-pressure bipolar membrane electrodialysis, Energy, Environ. Sci. 4 (2011) 4031–4037, https://doi.org/10.1039/c1ee01336j.
- [24] H. Nagasawa, A. Yamasaki, A. Iizuka, K. Kumagai, Y. Yanagisawa, A new recovery process of carbon dioxide from alkaline carbonate solution via electrodialysis, AIChE J 55 (2009) 3286–3293, https://doi.org/10.1002/aic.
- [25] A. Iizuka, K. Hashimoto, H. Nagasawa, K. Kumagai, Y. Yanagisawa, A. Yamasaki, Carbon dioxide recovery from carbonate solutions using bipolar membrane electrodialysis, Sep. Purif. Technol. 101 (2012) 49–59, https://doi.org/10.1016/j. seppur.2012.09.016.
- [26] R. Ramezani, S. Mazinani, R. Di Felice, State-of-the-art of CO2 capture with amino acid salt solutions, Rev. Chem. Eng. 38 (2022) 273–299, https://doi.org/10.1515/ revce-2020-0012.
- [27] M. Perumal, N.R. Karunakaran, A. Balraj, D. Jayaraman, J. Krishnan, A.B. J. Prakash, J. Arumugam, V.P. Muthukumar, Experimental investigation on CO2 absorption and physicochemical characteristics of different carbon-loaded aqueous solvents, Environ. Sci. Pollut. Res. 28 (2021) 63532–63543, https://doi.org/10.1007/s11356-020-10562-0.
- [28] R.E. Zeebe, D. Wolf-Gladrow, CO2 in seawater Equilibrium kinetics isotopes, ELSEVIER SCIENCE B.V, Amsterdam, 2001.
- [29] I.R. Salmón, N. Cambier, P. Luis, CO2 capture by alkaline solution for carbonate production: A comparison between a packed column and a membrane contactor, Applied Sciences (switzerland) 8 (2018), https://doi.org/10.3390/app8060996.
- [30] Z. Rastegar, A. Ghaemi, CO2 absorption into potassium hydroxide aqueous solution: experimental and modeling, Heat and Mass Transfer/waerme- Und Stoffuebertragung 58 (2022) 365–381, https://doi.org/10.1007/s00231-021-03115-9.
- [31] Q. Shu, M. Haug, M. Tedesco, P. Kuntke, H.V.M. Hamelers, Direct Air Capture Using Electrochemically Regenerated Anion Exchange Resins, Environ. Sci. Tech. 56 (2022) 11559–11566, https://doi.org/10.1021/acs.est.2c01944.
- [32] R. Sander, Compilation of Henry's law constants (version 5.0.0) for water as solvent, Atmos, Chem. Phys. 23 (2023) 10901–12440, https://doi.org/10.5194/ acp-23-10901-2023.
- [33] X. Wang, W. Conway, R. Burns, N. McCann, M. Maeder, Comprehensive study of the hydration and dehydration reactions of carbon dioxide in aqueous solution, Chem. A Eur. J. 114 (2010) 1734–1740, https://doi.org/10.1021/jp909019u.
- [34] A. Taqieddin, M.R. Allshouse, A.N. Alshawabkeh, Editors' Choice—Critical Review—Mathematical Formulations of Electrochemically Gas-Evolving Systems, J. Electrochem. Soc. 165 (2018) E694–E711, https://doi.org/10.1149/ 2.0791813jes.
- [35] R.P. Brent, An algorithm with guaranteed convergence for finding a zero of a function, Comput. J. 14 (1973) 420–425.
- [36] F. Barbir, Fuel Cell Electrochemistry, in: PEM Fuel Cells, 2nd ed., Academic Press, 2013: pp. 33–72. 10.1016/B978-0-12-387710-9.00003-5.
- [37] J.A. Harrison, A.T. Kuhn, THE ROLE OF GAS BUBBLE FORMATION IN THE ELECTRO-CATALYSIS OF THE HYDROGEN EVOLUTION REACTION, 1983.
- [38] E. Al-Dhubhani, R. Pärnamäe, J.W. Post, M. Saakes, M. Tedesco, Performance of five commercial bipolar membranes under forward and reverse bias conditions for acid-base flow battery applications, J Memb Sci 640 (2021), https://doi.org/ 10.1016/j.memsci.2021.119748.
- [39] S. Valluri, S.K. Kawatra, Reduced reagent regeneration energy for CO2 capture with bipolar membrane electrodialysis, Fuel Process. Technol. 213 (2021) 106691, https://doi.org/10.1016/j.fuproc.2020.106691.
- [40] R. Sharifian, R.M. Wagterveld, I.A. Digdaya, C. Xiang, D.A. Vermaas, Electrochemical carbon dioxide capture to close the carbon cycle, Energy, Environ. Sci. 14 (2021) 781–814, https://doi.org/10.1039/d0ee03382k.
- [41] R. Pärnamäe, M. Tedesco, M.-C. Wu, C.-H. Hou, H.V.M. Hamelers, S.K. Patel, M. Elimelech, P.M. Biesheuvel, S. Porada, Origin of Limiting and Overlimiting Currents in Bipolar Membranes, Environ. Sci. Tech. (2023), https://doi.org/10.1021/acs.est.2c09410.
- [42] M.A. Blommaert, J.A.H. Verdonk, H.C.B. Blommaert, W.A. Smith, D.A. Vermaas, Reduced Ion Crossover in Bipolar Membrane Electrolysis via Increased Current Density, Molecular Size, and Valence, ACS Appl Energy Mater 3 (2020) 5804–5812, https://doi.org/10.1021/acsaem.0c00687.
- [43] R. El Moussaouia, G. Pourcellyb, M. Maeck, H.D. Hurwitza, C. Gavachb, Co-ion leakage through bipolar membranes Influence on I-V responses and water-splitting efficiency, 1994.
- [44] M.J. Mitchell, O.E. Jensen, K.A. Cliffe, M.M. Maroto-Valer, A model of carbon dioxide dissolution and mineral carbonation kinetics, Proceedings of the Royal Society A: Mathematical, Physical and Engineering Sciences 466 (2010) 1265–1290. 10.1098/rspa.2009.0349.
- [45] A. Sáez, V. Montiel, A. Aldaz, An Acid-Base Electrochemical Flow Battery as energy storage system, Int. J. Hydrogen Energy 41 (2016) 17801–17806, https://doi.org/ 10.1016/j.ijhydene.2016.08.141.